Assessment of a color measurement-based method for the characterization of polymer thermo-oxidation.

Aurlien Doriat[a,*], Marco Gigliotti[a], Marianne Beringhier[a], Gildas Lalizel[a], Eva Dorignac[a], Patrick Berterretche[a], Matteo Minervino[b]

[a] *organization=Institut Pprime, CNRS, ISAE-ENSMA, Universite de Poitiers,addressline=1, Avenue Clement Ader, BP 40109, city=Chasseneuil Futuroscope, postcode=86961, country=France*
[b] *organization=Safran Aircraft Engine SAFRAN Group,addressline=Rond Point Rene Ravaud Reau, city=Moissy Cramayel Cedex, postcode=77550, country=France*

Abstract

Epoxy resins are used in various applications where environmental factors can interact and degrade the material. Thermo-oxidation is one of the degradation processes that can lead to both mechanical and chemical changes. This work aims to present a technique for characterizing thermo-oxidative degradation based on color analysis. The UV-Vis spectroscopy reveals the direct link between the chemical modification and the color variation. The color difference ΔE^*_{ab} between a virgin and an aged sample (in CIELAB color space) provides an excellent indicator of oxidation degree. Calibration correlations have been developed based on reference samples aged under known conditions of temperature and pressure, translating color differences into an oxidation equivalent duration, represented as an equivalent time t^* or to directly estimate mechanical properties. The t^* parameter is the time that the

*Corresponding author
Email addresses: aurelien.doriat@ensma.fr (Aurlien Doriat), marco.gigliotti@ensma.fr (Marco Gigliotti)

sample should be exposed to the reference conditions to undergo the same oxidation level (equivalent to the same color difference change and then, degradation). Nanoindentation measurements were performed to validate the color measurement method. Some limitations were identified, including the poor correlation under non-equivalent time-temperature-pressure conditions, poor relevance for assessing high oxidation levels, and the impact of light scattering in areas with strong color gradients. The spatial resolution of color measurement is ten times higher than nanoindentation. Furthermore, the color measurement is non-destructive, can be conducted in situ, and is suitable for monitoring the aging of industrial components.
Keywords: Thermo-Oxidation, Epoxy, Polymer Material, Yellowing, Color Measurement, UV-Vis Spectroscopy, Nanoindentation

1. Introduction

Polymers, including epoxy resin, have diverse applications in fields such as paints, adhesives, electronics, the biomedicine industry, and aerospace [1]. Given the often harsh conditions in which these applications are carried out, it is of paramount importance to be able to control the aging of polymers. The effects of humidity, UV radiation, and high temperatures can result in thermo-oxidation, which in turn leads to the degradation of polymers [2]. The present study will focus on the thermo-oxidation. Thermo-oxidation results in a modification of the chemical bonds, which consequently affects the chemical functional groups, leading to yellowing, for every polymer [3, 4]. The chemical alterations also result in mechanical changes : the balance between chain scission and crosslinking results into a shift of glassy temperature (and

the other phase transition) and the so called antiplasticization effet [5, 6, 7, 8, 9]. Consequently, the polymer becomes harder and the modulus of elasticity increases [6, 10, 7]. The embrittlement of the polymer alters the failure properties [8, 11].

The characterization of thermo-oxidation is based on the analysis of both chemical and mechanical changes. Approaches based on measuring mechanical properties allow to quantify thermo-oxidation at the local level. Nanoindentation is the preferred method by achieving elastic indentation modulus E_i measurements [12, 13, 14, 15, 16, 17, 18]. The indentation technique has been demonstrated to be an effective method for characterizing the thermo-oxidation processes, and is linked to chemical modifications. ([19, 11, 6, 20, 7, 21, 22, 23, 9]). The main disadvantages of this technique are related to its sensitivity to roughness (roughness should be 100 times smaller compared to the nanoindentation depth) or flatness (post-processing theory assumes axisymmetric contact between indenter and sample) [24, 25] . Additionally, the classical post-processing of nanoindentation data is a relatively complex issue due to their dependency on Hertz contact theory [26, 27, 28]. The spatial resolution of the indentation is constrained by the visco-plastic zone situated beneath the indenter. A general guideline suggests that each measurement should be spaced a minimum of 6 times the indentation depth which lead to a spatial resolution of at least 12 µm.

Alternative methodologies based on color change have been developed. The reaction of oxygen with polymer chains results in new chromophoric functional groups, including conjugated carbonyls, causing yellowing. These chemical changes have been extensively investigated in photo-oxidation ([29,

4]) but the underlying mechanisms appear to be analogous to those observed in thermo-oxidation ([30, 31, 4]). The mechanisms of yellowing in amine curred epoxy is discussed in [32]. While the precise carbonyl functional group remains undetermined [33], the quinone methide group is thought to be a prominent contributor in aromatic epoxies [31, 34, 4]. Additional groups, in too small quantities to be detected, may also be involved such as hydroxyl group or double carbon bond [4, 30].

Yellowing has been broadly identified, but only a limited number of studies have employed it as a quantitative measurement to characterize thermo-oxidation. Two quantities have been used. First, the yellowing index (which converts a color tristimulus into one quantity) and its variation provides an insight into the color change [4]. Subsequently, the color difference (which is an Euclidean norm in the CIELAB color space) has been utilized to quantify the color change [29, 35, 36, 37]. Some authors ([29, 36]) have demonstrated that these quantities are suitable for describing thermo-oxidation due to their correlation to physical changes. Indeed, the color-based quantity exhibits analogous behaviors to those observed in the more classical thermo-oxidation characterization method ([36]). For example, linear dependency has been proven ([29]) between color difference and imide (carbonyl group) absorption band ratio. The close relationship between thermo-oxidation chemistry and color change is well established ([4, 29, 36]). Consequently, color change can be employed as an oxidation tracer. Previous studies ([36]) have shown the relevance of this parameter for studying heterogeneous oxidation.

However, none of these techniques correlates the color change to the mechanical properties. Furthermore, the color difference is highly dependent on

lighting conditions. In this paper, we propose an optical technique for qualifying the degree of local oxidation based on the color change. This allows avoiding one of the main drawbacks of nanoindentation, that is high dependency on surface roughness and relatively poor spatial resolution. Following the characterization of the reference samples, each color change measurement is related to an equivalent oxidation level in the reference conditions (via an equivalent time). This is done in order to establish a direct relationship between the color change and the oxidation level. If the mechanical or chemical properties of this oxidation level are known, then these quantities can be measured indirectly. Here, the proposed method will be validated with indentation measurements, for samples aged under various temperature and pressure conditions.

Firstly, a study of the reflection spectrum from the polymer under several light sources will be carried out to link chemical modifications to color changes in section 3. Secondly, a method based on color change will be developed to characterize the degree of thermo-oxidation of a polymer in section 4. In conclusion, this technique will be validated based on comparison with elastic indentation modulus and the main limitation will be discussed in section 5.

2. Experimental set up

2.1. Materials and aging

An aromatic diamine epoxy resin is used in this work. It is chemically close to the DGEBF-CAF resin and the PR520 resin made by Cytec Engineered Materials used in the aerospace industry (see [18, 38, 39, 40]). Samples

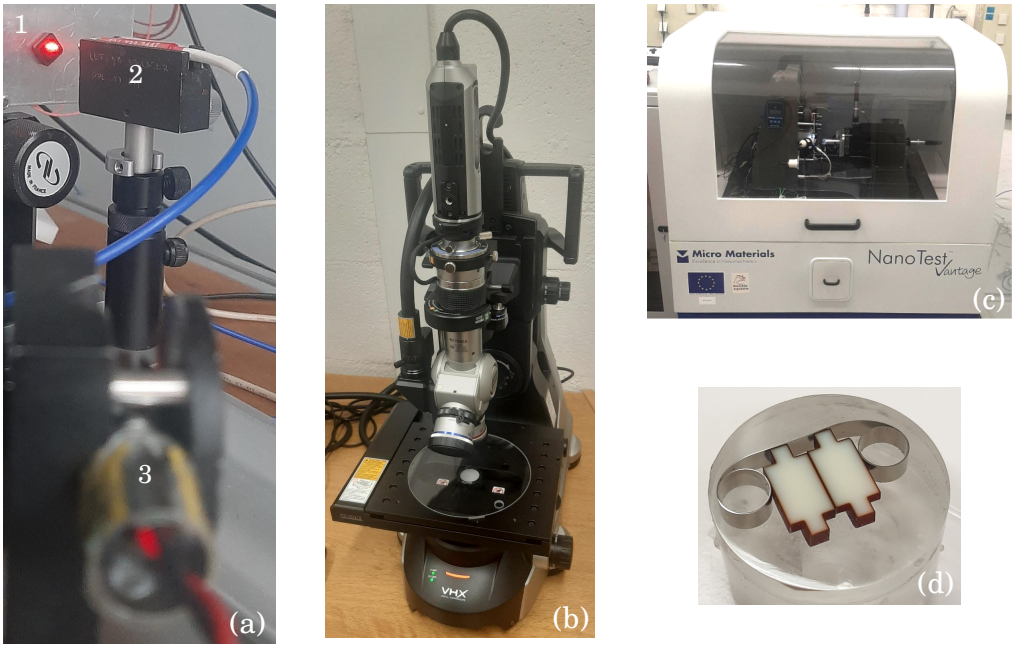

Figure 1: (a) UV-Vis spectroscopy experimental set up : the LASER (3) illuminates the sample (1) and the reflective light is measured by the spectrometer (2). (b) VHX-7000 microscope used for color measurements. (c) NanoTest Vantage nanoindentation machine. (d) Cutted, coated and polishing sample.

have been produced by SAFRAN and received as 5 mm thick parallelepipedic blocks, and the total exposed surface area is 16 mm^2.

The samples were exposed to atmospheric air conditions at 150 °C in an oven for durations ranging from 10 h to 1000 h. The ventilation oven is set to a level where the oxygen is renewed and no flow is created around the sample.

2.2. UV-Vis spectroscopy

The reflective spectra from three distinct light sources have been measured in order to link oxidation with the color variation. The spectra are obtained with a USB4000 spectrometer with an optical fiber from OceanOptics. The device is capable of counting the number of photons for each wavelength between 350 nm and 1000 nm with a spectral width accuracy under 2.3 nm. The light reception from optical fiber is oriented at an angle of ,45° from the sample surface to limit direct reflection. The experimental setup is shown in Fig. 1(a).

The reflective spectrum is highly dependent on the light source as the intensity measured is proportional to $I_{light}(\lambda)\rho(\lambda)$ with $I_{light}(\lambda)$ the intensity of the light source and $\rho(\lambda)$ the reflectivity of the sample. In this study, four light sources were used. The first two ones are continuous to study the variation of reflection according to wavelength. The first one is a halogen lamp with type J bulb of 500 W. The integration time of the spectrometer is set to 500 ms to maximize the spectrum amplitude. The lengthy integration time results in a noisy curve, so the data is smoothed with a Savitzky-Golay filter (window of 51 points and polynomial of order 1). The second continuous light source is the annular LED lamp of the Feyence VHX-7000 microscope

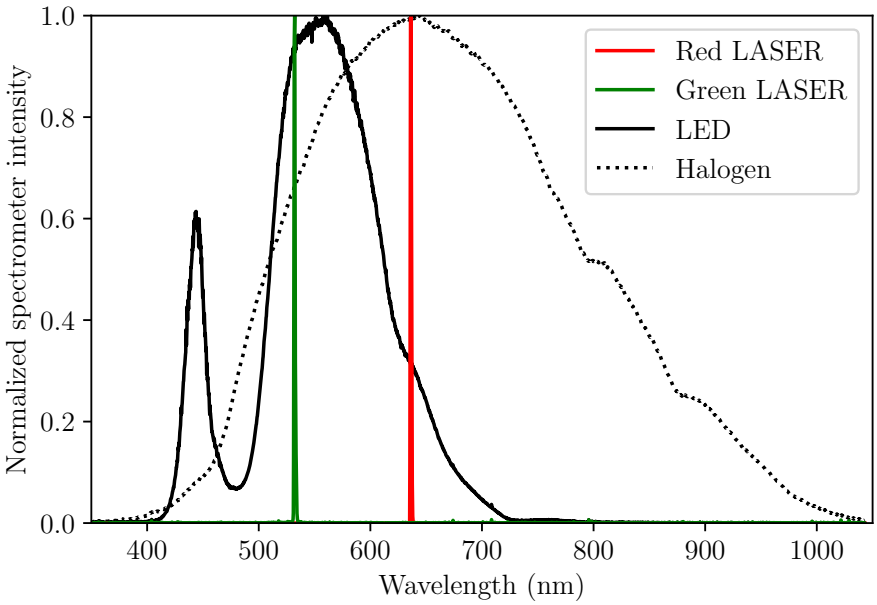

Figure 2: Light sources reflective spectra on virgin sample.

used to image the sample. This light source is used to emphasize the equivalence between spectroscopy and color measurements. For this light source, the integration time is set to 100 ms and no filtering is needed to smooth the spectrum. The last two light sources are LASERs. The green LASER is an EverGreen which emits 2 pulses at 25 Hz at $\lambda = 532$ nm with power of 100 mJ. The integration time is set to 100 ms (4 pulses are measured). Due to the intensity variation between the laser pulses, a study spectrum is the average of 50 spectra. The red LASER is a diode from AMS electronic emitting at $\lambda = 635 \pm 5$ nm with a power of 4 mW. Because of the high power, the integration time is 3 ms but the intensity maximum changes a lot with respect to time, so the spectrum is averaged over 2000 measurements.

Fig. 2 displays the emission spectra of all light sources reflected on the virgin epoxy sample. Each spectrum is normalized by the maximum number of photons received with the virgin sample to enable comparison between them, as the maximum intensity varies between light sources. The halogen bulb produces a broader spectrum, including near-infrared wavelengths. The LED source exhibits two peaks that correspond to the sensitivity of the eye cones. Although calibrated to appear white, this light source is crucial for linking spectroscopy and color difference measurement. Additionally, the two lasers are monochromatic sources.

2.3. Color measurement from images

Color measurements have been realized from images obtained with an optical microscope Feyence VHX-7000 (Fig. 1(b)) with a dual lens with a magnification of 20. It is possible to obtain a higher resolution, but it has been chosen to have one image for the whole sample to avoid rebuilding the image.

The microscope camera has a CMOS sensor with a high accuracy resolution of 6144×4608 pixels, resulting in a spatial resolution of 2.5 µm per pixel. Each pixel has a dynamic range of 16 bits. The luminosity (integration time) is set to 4 ms with an annular light to have the virgin sample the most white and, at the same time, the more oxidized sample dark. The idea is to work with the wider color dynamic and then maximize the color difference between the virgin sample and the oldest of the study. This light is also more homogeneous than the axial light source.

Before taking a picture of the surface, the sample does not undergo any surface preparation. All the images are saved in TIFF format in RGB without

any compression treatment.

2.4. Elastic indentation modulus measurement

Nanoindentation measurements have been performed on a NanoTest Vantage machine from MicroMaterials (Fig. 1(c)). Samples were prepared by cutting them in half, then putting them side by side, bound by an elastic band, and finally coated (Fig. 1(d)). The preparation aimed to limit the edge effect when indenting near the interface by adding coated resin on the other side of the interface. The measurement surface was polished to reduce the roughness below 10 nm and to limit the effect of surface variation on nanoindentation measurement (see [18, 41] for more details about sample preparation).

Nanoindentation tests were performed with a spherical indenter of 5 µm radius. Tests were controlled in force until a maximal force of 5 mN was applied for a duration of 20 s because of the visco-elastic behavior of the polymer. The velocity of the load and unload phase was set to $0.5\,\mu m\,s^{-1}$. The data recorded during the unloading phase was used to process the reduced elastic indentation modulus E_{red} (Eq. 1) with the method of Oliver and Pharr [27] :

$$E_{red} = \frac{\sqrt{\pi}\frac{dF}{dh}}{2\beta\sqrt{A_p}} \tag{1}$$

with $\frac{dF}{dh}$ being the slope at the beginning of unloading, A_p the surface contact between the indenter and the sample, and β the indenter geometrical parameter ($\beta = 1$ for a revolution indenter). Based on the properties of the indenter, the elastic indentation modulus E_i is estimated (Eq. 2) :

$$\frac{1}{E_{red}} = \frac{1-\nu_{ind}^2}{E_{ind}} + \frac{1-\nu_{poly}^2}{E_i} \tag{2}$$

with $E_{ind} = 1141\,\text{GPa}$ and $\nu_{ind} = 0.07$ the elastic modulus and Poisson coefficient of the diamond indenter and $\nu_{poly} = 0.4$ the Poisson coefficient of the polymer. The oxidized layer is characterized by elastic indentation modulus profile. One profile is a discrete measurement 5 µm from the edge of the sample and every 15 µm. This experimental profile is repeated 10 times (every 50 µm). Each profile shown in this study is the mean profile of these 10 profiles. The vertical error bar is the value of one standard deviation (measurement uncertainty is at least 10 lower than the variation between measurements).

3. Visible reflective spectroscopy

The analysis of visible reflective spectroscopy allows better understanding the chemical analysis discussed in the literature. Fig. 3 shows the reflective spectra for virgin and aged samples between 10 h and 1000 h at 150 °C from the LED source light. Fig. 4 illustrates the reflective spectra using the halogen light source. The same conclusions apply regardless of the light source.

Information about the absorption is linked to the reflective and transmission spectra. The samples are assumed partially opaque so the transmission is close to zero. Then, if the reflectivity ratio decreases, the absorption increases ($\rho + \tau + \alpha = 1$ with ρ the reflectivity, α the absorbtivity and τ the transmitivity). As a first order approximation, transmissivity is assumed to be zero. This hypothesis is discussed in section 5.4.

First, when the aging duration increases, the number of photons received by the sensor decreases for all the wavelength, illustrating the samples' darkening. The maximum is also slightly shifted to the yellow/red wavelength,

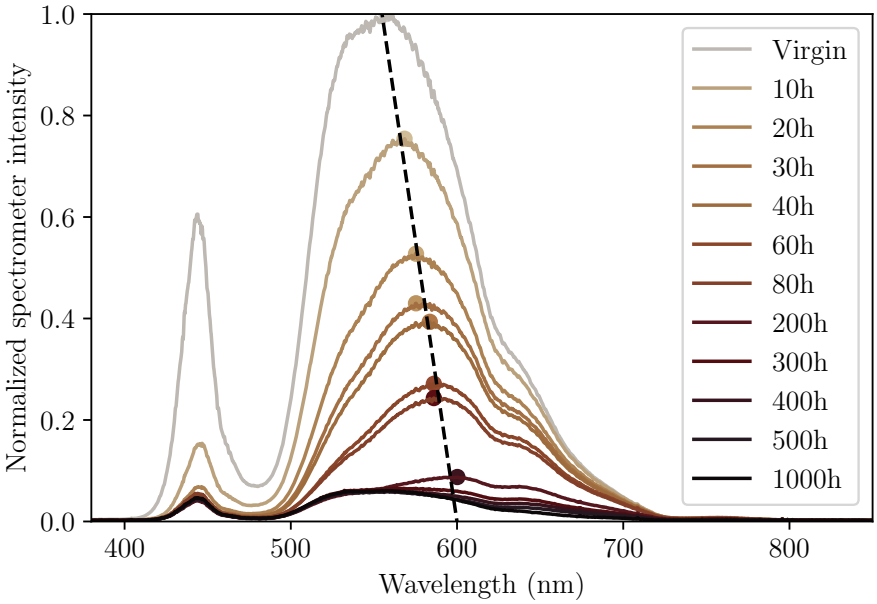

Figure 3: Raw reflective spectra from LED light for samples aged at 150 °C. As the exposure duration increases, the absorption increases and the reflective intensity decreases.

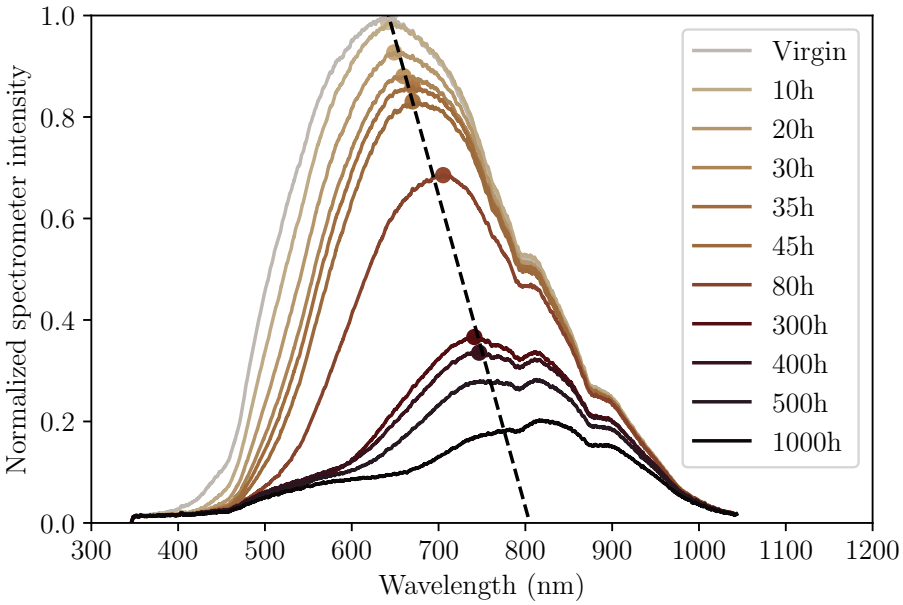

Figure 4: Raw reflective spectra from halogen light for samples aged at 150 °C. The oxidation increases the absorption, so the reflective intensity decreases, but less rapidly with the halogen light source than with the LED one because the maximum emission is closer to the red wavelength.

which is the yellowing (also called "browning ") of the samples. The absorbtivity increases quickly around 450 nm by the creation of quinone methide groups, as [31] has already mentioned on aromatic diamine epoxy (seen by [30] before). This article aims not to identify the function group that creates this yellowing but to use it as a measure of degree of thermo-oxidation aging. Finally, the maximum of the peaks of the reflective spectra is linearly interpolated. All the maxima of the spectroscopy spectrum belong to this line even if the sample is aged at different temperatures. Indeed, Fig. 5 shows the variation of the normalized spectrometer intensity against the maximum's wavelength spectrum. The data at 150 °C are the maximum of the spectra plotted on Fig. 4. Data from two aging temperatures (140 °C and 150 °C) and different aging duration (between 10 h and 100 h) are represented but all the maxima belong to the same line. This demonstrates that temperature is an accelerating factor in the color change process and so in the oxidation. Regardless of the temperature, the exposure duration can be adjusted to achieve the same color change. The maxima remain on the same slope, indicating that the yellowing is only a function of the degree of oxidation. In other words, for a given color, the time-temperature couple can be adjusted to obtain the desired result.

A reflectivity ratio R is defined (Eq. 3) to move towards integrated color criteria as :

$$R = \frac{\int_{\lambda_{min}}^{\lambda_{max}} N_s(\lambda) d\lambda}{\int_{\lambda_{min}}^{\lambda_{max}} N_v(\lambda) d\lambda} \tag{3}$$

with $N_i(\lambda)$ the intensity received from the spectrometer (proportional to the photon number between 1 and 2^{16}) at a given wavelength λ, s is an aged sample and v is the virgin sample (used as a reference). λ_{min} and λ_{max} are

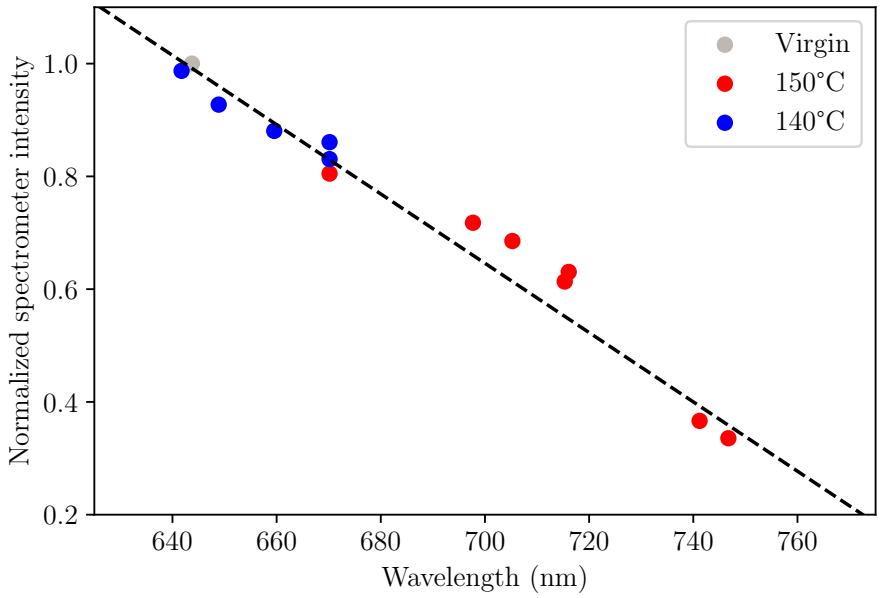

Figure 5: Maxima coordinates (normalized spectrometer intensity against wavelength) of spectrum for two different aging temperatures (150 °C and 140 °C) and aging duration. The data at 150 °C are the maximum of the spectra plotted on Fig. 4. This plot proves that the temperature is an accelerating factor of oxidation as the same linear dependency is noticed.

Light source	λ_{min}	λ_{max}
LED	300 nm	800 nm
Halogen	300 nm	800 nm
Red LASER	631 nm	639 nm
Green LASER	530 nm	535 nm

Table 1: Summary of λ_{min} and λ_{max} for the four light sources.

the wavelengths limits of the light source. The value for the light sources are in Tab. 1.

For the green LASER, the other wavelengths than $\lambda = 532$ nm are only due to the spectrometer precision.

Fig. 6 shows the variation of R as a function of aging duration for four distinct light sources : a LED source, a halogen source and two lasers. Two regimes can be seen distinctively. In all cases, the reflectivity ratio R decreased with increasing aging time, which is consistent with the browning of the sample over time. The ratio R remains constant for a given light source after a certain time interval, which we define as the variation limit time (Vt). For instance, the ratio R is observed to remain constant after 300 h when illuminated by the red LASER light source and after 100 h when illuminated by the LED light source. The LED and halogen light sources emit light continuously, yet their respective wavelength ranges differ. The halogen light source illuminates at least until 1000 nm (maximum range of the sensor), whereas the LED light source illuminates until 720 nm (see Fig. 2). The halogen light source emits in the near-infrared region, resulting in a higher sensitivity than the LED light source.

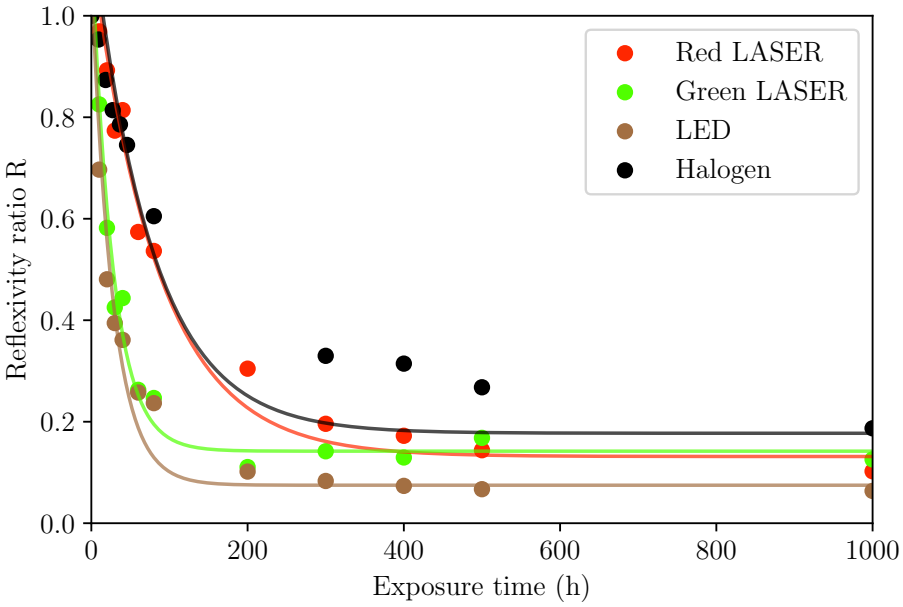

Figure 6: Reflexivity ratio R over the exposure time for three different light sources. The exposure time to reach the asymptotic value depends on the light source. So is the sensitivity range of the measurement.

The decrease of R with the aging duration has been interpolated by Eq.4 with the two parameters τ and R_∞.

$$R(t) = e^{-\frac{t}{\tau}} + R_\infty \tag{4}$$

This interpolation function represents the solution of a first-order differential equation with τ the time constant. Subsequently, the reflectivity ratio R furnished data until the variation time limit V_t is reached : $V_t = -3\tau$. This limit is defined as three times the time constant of a first-order linear time invariant. The variation time limit is the exposure duration at under specified aging conditions until which the color variation can be calculated before remains constant, once color change has ceased. In this context, the reference conditions are defined as follows : $T = 150\,°\mathrm{C}$ and $P = 0.21\,\mathrm{bar}$. The variation time limit V_t has been calculated for each wavelength based on the reflective spectra obtained through the use of a halogen lamp (the broader along the wavelength range). Fig. 7 shows that the variation time V_t increases is smaller as the wavelength increases. The value of the variation time V_t can be estimated from Fig. 6 for the two LASER wavelengths around 100 h for the green LASER and 300 h for the red LASER. The values shown in Fig. 7 are based on the halogen light source and are similar to those estimated previously.

Therefore, the lighting source used to estimate the reflectivity ratio R will be selected based on the variation time limit V_t needed.

On the one hand, the bounds of the integral in R should remain relatively small (for example, lower than 550 nm) to be precise at small aging duration, while for the characterization of longer aging durations, the higher

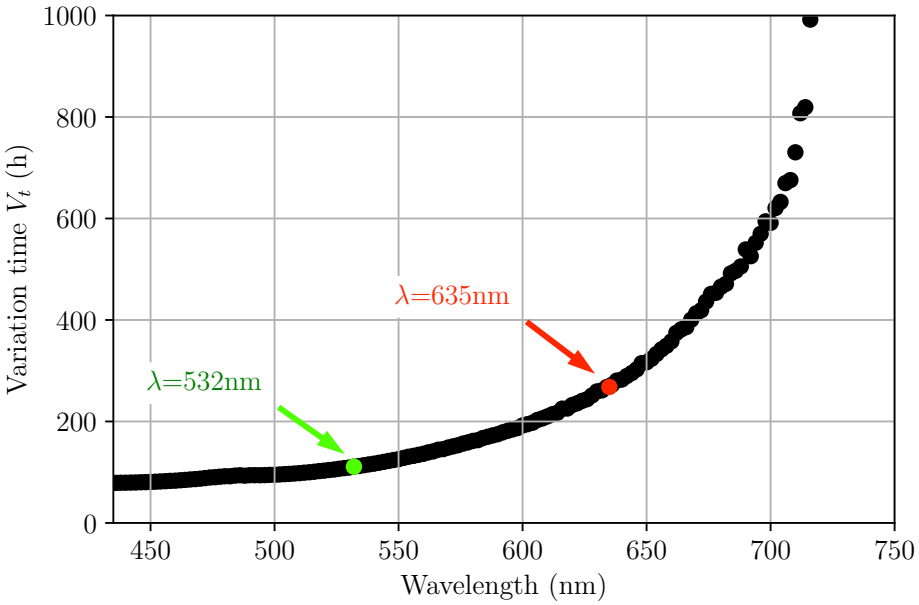

Figure 7: Variation time limit V_t is a function of the wavelength. All the data have been calculated from the halogen light source. The variation time is the exposure time until the absorbance does not vary enough to make a measurement. This time is function of the wavelength, so the light source.

wavelength is preferred (for example, higher than 650 nm).

On the other hand, illuminating light can be chosen with a narrow wavelength range (such as LASERs) depending on the sensibility and the maximum aging duration studied. The choice of the wavelength will directly impact the sensitivity range of the color or spectroscopy measurements.

Ultimately, the integrated reflectivity ratio R can be used as a characterization method of the thermo-oxidation degree.

Spectroscopy and color difference measurements are linked. Each wavelength represents a specific color, and a reflective spectrum indicates the contribution of each color to the color perceived by the human eye (and camera). The integration of all wavelengths within the spectrophotograph ultimately yields a single color, contingent upon the number of photons present for each wavelength. Therefore, the color of the samples studied presented in the next section is directly linked to chemical changes induced by thermo-oxidation with high spatial resolution. Moreover, it represents a rapid and non-destructive measurement technique.

4. Aging characterization based on the color measurement from images

The proposed method is based on color difference measurements. The objective is to characterize the thermo-oxidation for one condition of temperature and oxygen pressure defined as the reference conditions. Subsequently, by establishing correlations between the color difference and the time or the mechanical properties (or any measured properties), it would be possible to know the oxidation state of any given sample that has undergone aging under

other conditions or in a complex environment.

4.1. Color difference measurement

A digital image of the sample is captured in TIFF format, and the color coordinates are extracted pixel by pixel. The picture is saved in standard Red, Green, and Blue coordinates (sRGB). This color space has been developed based on the three types of cone eyes, which are sensitive to short, medium, and long wavelengths (i.e. blue, green, and red). In 1931, the International Commission on Illumination (CIE) established the RGB color space. During the same convention, the Commission Internationale de l'clairage (CIE) defined a tristimulus value, designated XYZ. This final color space encompasses all color variations that can be discerned by the human eye. It should be noted, however, that the primary colors of this color space are not within the visible range. Then, the most evolved color space was defined in 1976 by the CIE with the CIELAB color space. L^* is the lightness, a^* a parameter between green and magenta and b^* a parameter between blue and yellow. This color space is dependent upon the four colors that humans are able to perceive, and it is a quasi-uniform space. This indicates that a variation in the parameter results in the same variation in eye color. This color space is selected for the calculation of color differences due to its uniformity property.

Formulas have been developed to facilitate the conversion between different color spaces, with the CIE defining the coefficient value in this context. In this study, the OpenCV Python library was employed for the conversion of RGB to LAB. The conversion function is based on the sRGB standard with a white reference of D65. It should be noted that the images were not captured

with this specific light reference, which may result in discrepancies between the final CIELAB value and the color difference value and the established standards. Nevertheless, the value remains meaningful, particularly given the objective of conducting a comparative analysis between images of virgin and aged polymers.

The initial definition of the color difference ΔE was introduced in 1976 by CIE. It is an Euclidian norm (Eq. 5) inside the CIELAB space defined as (v for virgin sample and s for aged sample):

$$\Delta E^*_{ab} = \sqrt{(L_v - L_s)^2 + (a_v - a_s)^2 + (b_v - b_s)^2} \tag{5}$$

The human eye can see the difference between two colors from $\Delta E^*_{ab} = 2$.

Fig. 8a shows an example of an image of the color difference calculation ΔE^*_{ab} for a 80 h aged sample. The CIELAB coordinates of the virgin sample are averaged from all the values measured on the sample surface. The mean virgin CIELAB coordinates are (73.7, 0.5, 3.7) ± (0.6, 0.4, 0.4). These values can range between 0 and 100 for L^* coordinate and between -127 and 128 for a^* and b^*. The variation of the color in the virgin sample is due to slight difference in the materials. This results in a variation of $\Delta E^*_{ab} = 0.8$. Then, the color difference is calculated between each pixel CIELAB value of the aged sample and the virgin averaged CIELAB values. It is recommended to average the white before making the color difference, to avoid multiplying errors, as would be the case with a pixel by pixel color difference. Here, the surface is homogeneous and the advantage of averaging the reference (virgin) sample is being able to make the color difference of samples with different shapes than the reference. In this study, the samples used for the validation with nanoindentation measurements have a different shape as the

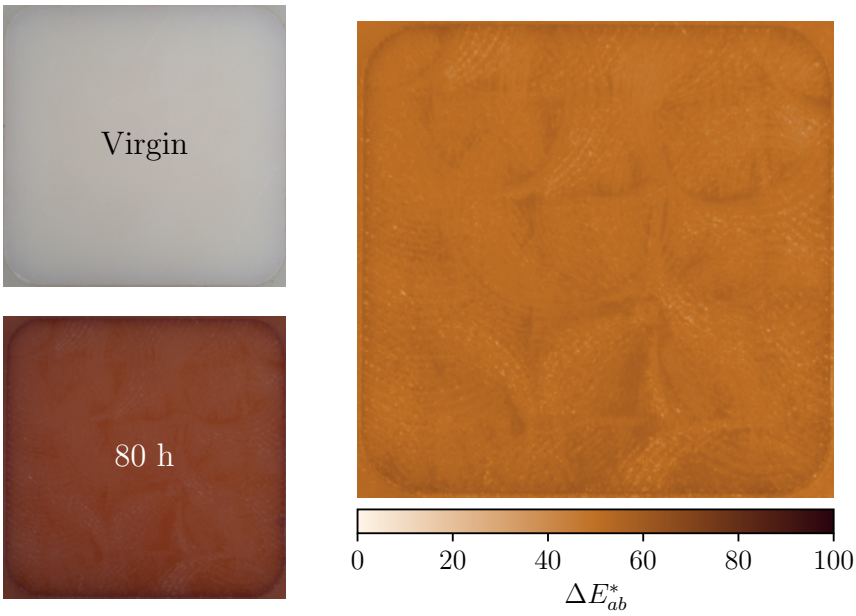

(a) ΔE^*_{ab} map calculation for 80 h aged sample at 150 °C. As the maximum of color change with our epoxy resin is 71, this sample has reach almost two third of its color change and so close to two third of its oxidation.

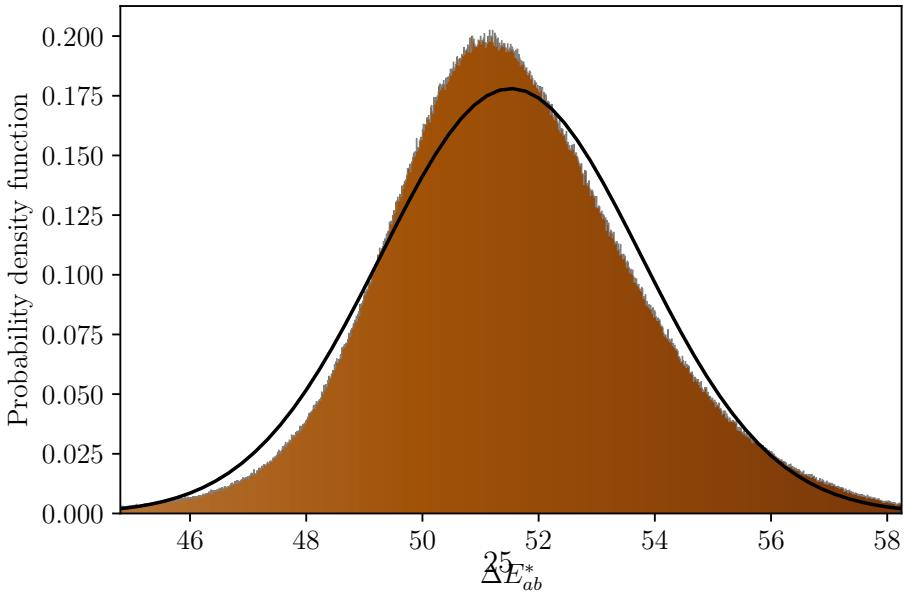

(b) ΔE^*_{ab} distribution for 80 h aged sample. The black line is the comparison with a Gaussian distribution with the same mean and standard deviation.

Figure 8: ΔE^*_{ab} analysis for 80 h aged sample at 150 °C.

nanoindentation and color measurements are made in the cross section of the sample to identify the oxidized layer. The color difference calculation results in a map of ΔE^*_{ab} with the same spatial resolution as the picture (i.e. 2.5 µm). The aged sample is considered homogeneous (because it is aged in an oven with homogeneous temperature and air conditions) enough to plot the probability density function of the color difference shown in Fig. 8b with $\sqrt{N}$ bins number with N the number of pixels used to estimate the histogram. The probability density function is centered to the mean and the range is 6σ with σ the standard deviation. Then, the values of the mean and the standard deviation are : $\Delta E^*_{ab_{80h}} = 51.5 \pm 2.2$. The black curve is a Gaussian distribution function on the same plot with the previous average and standard deviation. The good agreement validates the homogeneous hypothesis of the color of the aged sample.

On Fig. 8a, surface imperfection can be noticed even for a homogeneous oxidized sample. This is due to the reflection of the light on the small surface's roughness. This is a factor influencing the standard deviation of ΔE^*_{ab}. For homogeneously oxidized samples, the use of a Gaussian filter can be advantageous in reducing this standard deviation while preserving the average value. This filter has one parameter ϕ that controls the smoothing effect. The filter size is set to 4ϕ.

Fig. 9a shows a ΔE^*_{ab} map filtered with a Gaussian filter with $\phi = 100$ and kernel size of 400 px. Compared to Fig. 8a, the result is a blurred map. Fig. 9b shows the effect of the parameter ϕ on the ΔE^*_{ab} mean and standard deviation for the 80 h aged sample. As the filter is centered, the mean value remains constant but the standard deviation decreases quickly. The standard

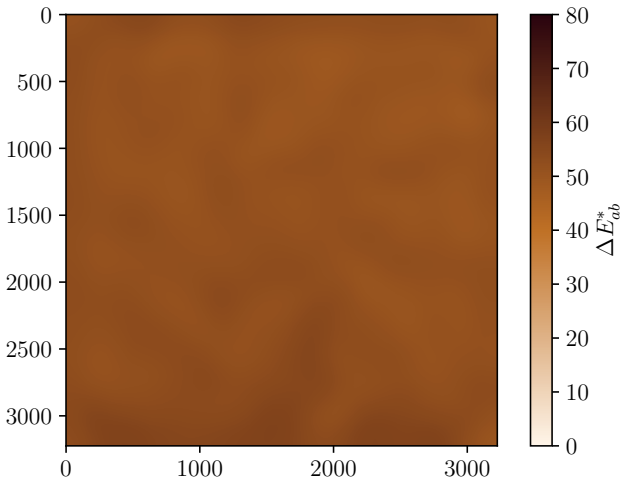

(a) ΔE^*_{ab} map filtered with a Gaussian filter with $\phi = 100$ and kernel size of 400 px at 150 °C

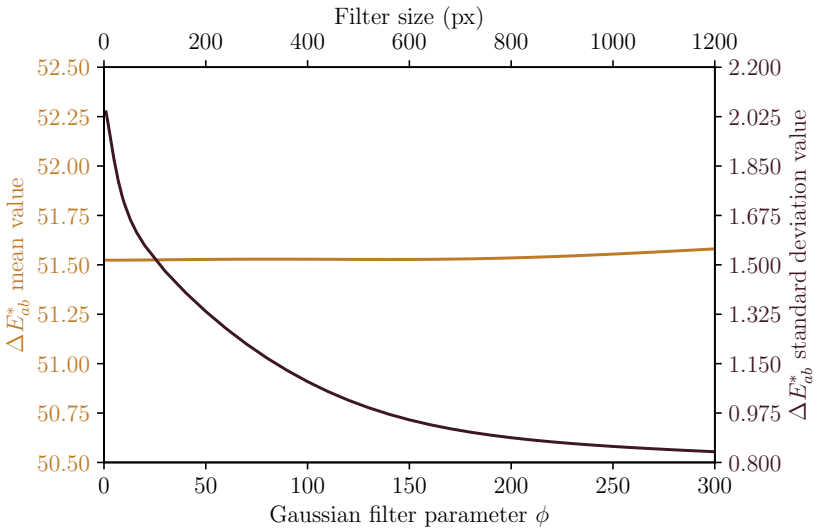

(b) Parametric study of the effect of value of ϕ on the mean and standard deviation of ΔE^*_{ab} for 80 h aged sample at 150 °C.

Figure 9: Effect of Gaussian filter on ΔE^*_{ab}.

deviation with $\phi = 100$ is two times lower than the original measurement. The drawback is the loss of spatial resolution due to the filter window size. In the following, a Gaussian filter will be applied to homogeneously oxidized samples if the standard deviation is over 2 (human eye). In this case, the parameter ϕ is set to 30 (with a kernel size of 120 px).

In addition to the color difference variability on the same sample, the absolute uncertainty due to the color variation between two identical samples is around $\Delta E^*_{ab} = 1$. This was evaluated by comparing three virgin samples. This means the measurement is reproducible.

4.2. Establishment of calibration correlations from reference aging conditions

This step aims to link the color difference ΔE^*_{ab} to the equivalent time t^* and indentation modulus E_i. Samples aged in reference conditions are characterized to establish these correlations. Here the reference condition is an aging temperature of 150 °C at atmospheric pressure. From these correlations, the oxidation state of a sample aged in a different environment can be determined only by a color difference measurement.

Samples aged from 5 h to 1000 h are characterized by measuring color difference and indentation elastic modulus. Fig. 10 shows the color change for some samples aged at reference conditions due to thermo-oxidation. The effect of thermo-oxidation on yellowing has already been shown ([30, 31, 29, 32, 4]). With the studied material, a similar yellowing effect is noticed. First, the color difference range is more than ten times superior to its standard deviation, which validates this parameter as the sensitive physical quantity. The sample became brownish as the exposure time increases and the color difference value increased simultaneously. As seen before with the spectroscopy

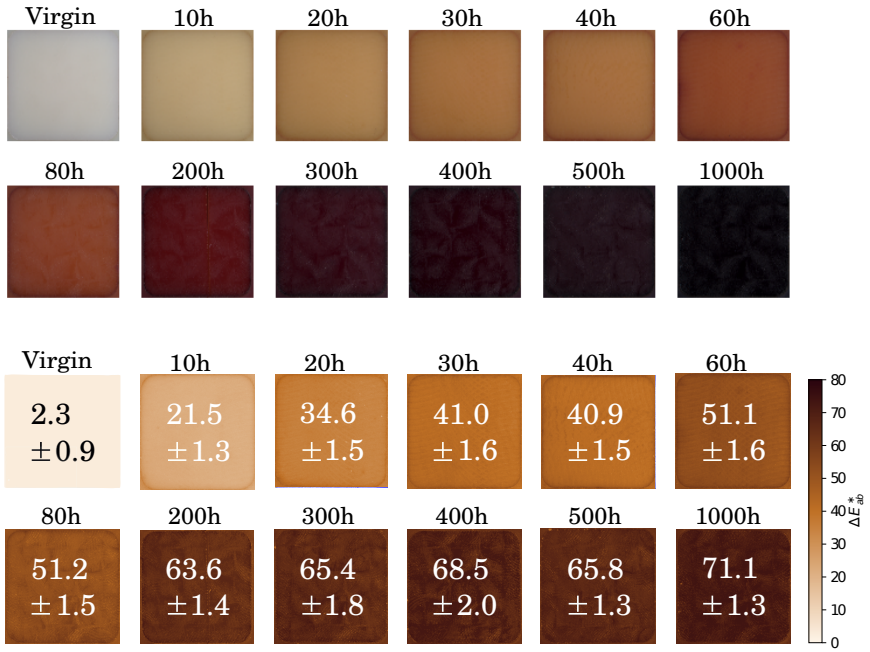

Figure 10: Raw images (top serie) and color difference map (ΔE^*_{ab}, bottom serie) measurement for aged samples at reference condition ($T = 150\,°\mathrm{C}$ and $P = 0.21\,\mathrm{bar}$).

results (see Fig. 6 for instance), from 300 h the value remains constant (under the range of the standard deviation).

The color difference ΔE^*_{ab} and the spectrometric reflexivity ratio R are plotted in Fig. 11 for the LED light source. The correlation between these two quantities validates the equivalence in the characterization of thermo-oxidation between spectroscopy and color difference measurement since linear correlation can be used to go from one characterization to the other regardless of the exposure time at the same aging temperature. It shows that the color difference is directly linked to the variation of radiative absorptivity due to the chemical modifications correlated to oxidation of polymer and thus to chemical alteration during thermo-oxidation.

This article does not investigate the origin of color change; rather, it employs color change as an oxidation tracer. The improvement with the presented method compared to existing methods ([29, 35, 36, 37]) is to link the color difference to a mechanical parameter or determine a shift factor. This is possible by determining correlations between parameters at reference aging conditions.

The main drawback of working with the color difference is its sensitivity to the source light and, more generally, to the experimental setup. We suggest a calibration correlation from reference samples (aged under reference conditions and for a known duration) to overcome these drawbacks as this correlation eliminates all the dependencies on the setup, allowing us to work with a parameter that only depends on the sample and its oxidation level.

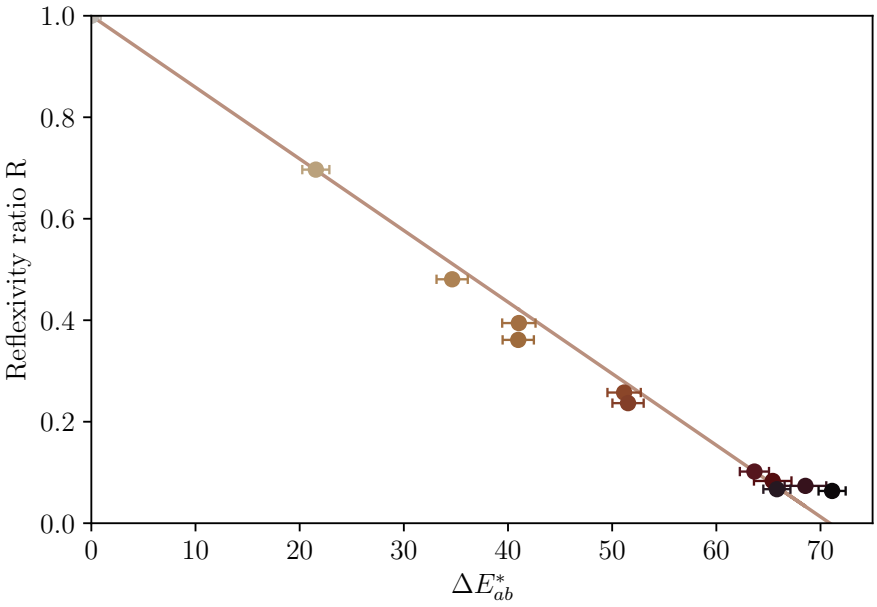

Figure 11: Comparison between color difference ΔE^*_{ab} and spectroscopy measurements R. The two measurements are corresponding as the linear dependency is noticed for different oxidation state denoted by the color of the data on the plot. (See Fig. 3)

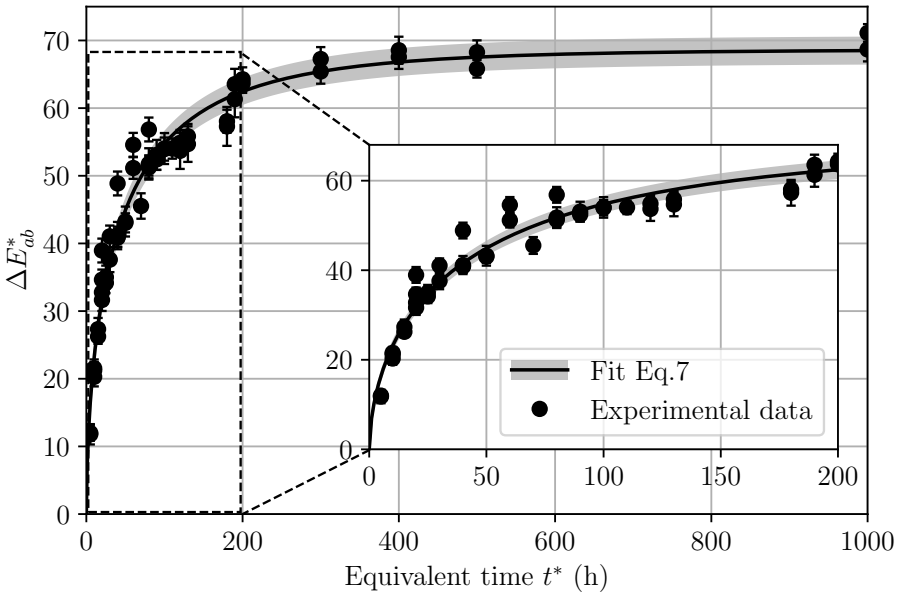

Figure 12: Correlation between the color difference ΔE^*_{ab} and the equivalent time t^*. The equivalent time t^* is the exposure time for samples aged in the reference conditions. The correlation data derived from samples that had been aged in the reference conditions only.

4.2.1. Correlation between color difference ΔE^*_{ab} and equivalent time t^*.

In order to establish the first correlation, color difference of sample aged at reference conditions have been measured and plot against their exposure time.

Fig. 12 shows the correlation between the color difference ΔE^*_{ab} and the equivalent time t^*. This parameter t^* is defined as the exposure time for samples aged at reference conditions ($P_{O_2} = 0.21\,\text{bar}$ and $T = 150\,°\text{C}$). In other aging conditions, it is the time that a sample should be exposed to the reference conditions to obtain the same color difference, therefore the same

oxidation state. From this equivalent time, a shift factor a_T which describes the acceleration or the slowdown of the thermo-oxidation is defined by Eq. 6 as in [42].

$$t^* = a_T t \tag{6}$$

where t is the real exposure time under various aging conditions. This shift factor has already been used ([42, 43, 44, 45]) to determine equivalence between time, temperature and pressure in thermo-oxidation process. The shift factor was defined and estimated when the aging conditions are homogeneous (constant temperature and pressure), the advantage of the equivalent time is its ability to still estimate the shift factor when the aging environment changes over time (variable temperature or pressure). The color difference increases rapidly at the beginning because the chemical oxidation reactions are self-accelerating until the number of oxidation sites is reduced, then the reactions slow down and the color difference changes more slowly. The experimental data have been fitted with Eq. 7. The shape of this correlation was chosen to model the saturation phenomenon of the thermo-oxidation and acceleration phase at the beginning. More precisely, the function is derived from the solution of a first order chemical reaction that can model the thermo-oxidation but a power is added over time to improve the fit. This kind of empirical model is used to model oxidation ([46, 47, 48]).

$$\Delta E^*_{ab}(t^*) = a\left(1 - e^{-bt^{*^c}}\right) \tag{7}$$

with $a = 66.8$, $b = 0.09$ and $c = 0.64$ the three adjustable parameters.

Thanks to the correlation in Fig. 12, from any color difference measurement, is possible to estimate an equivalent time and therefore a shift factor.

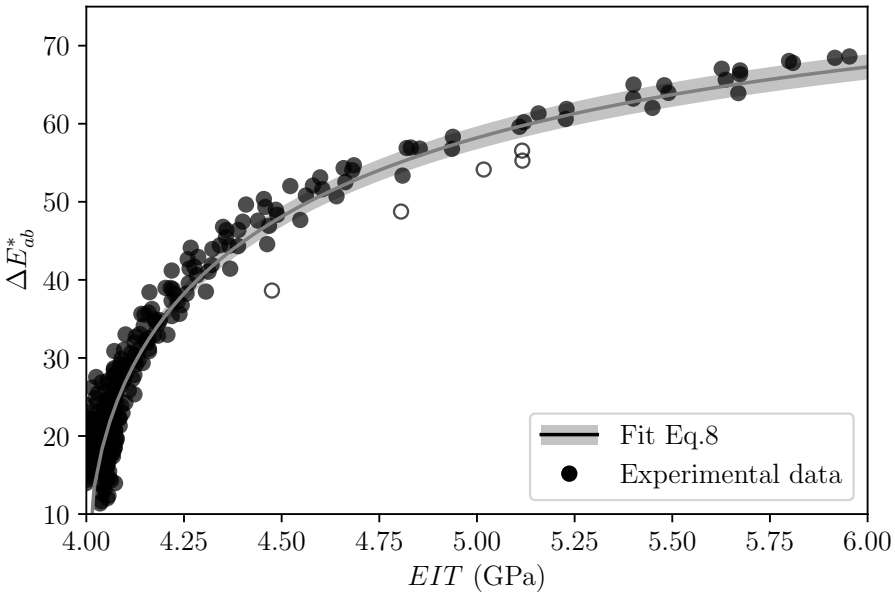

Figure 13: Correlation between the color difference ΔE^*_{ab} and the indentation elastic modulus E_i. The points closest to the edge are unfilled because they are subject to the edge effect (discussed later), which falsifies the measurement. The correlation data derived from samples that had been aged in the reference conditions only.

4.2.2. Correlation between color difference ΔE^*_{ab} and elastic indentation modulus E_i

In the case where the user needs to link directly the color difference to the mechanical properties, a correlation between these two quantities can be established while the mechanical quantities are measured on the reference samples.

Fig. 13 shows the correlation obtained. The correlation data were derived from indentation and color difference profiles within the sample, which were

obtained from samples that had been aged in the reference conditions. Regardless of the exposure time or the position in the oxidized layer, one color change corresponds to to one mechanical property. The shape of the correlation shows that the kinetics of color change and indentation modulus are not the same. This is consistent with the fact that the kinetics of carbonyl formation are different from those of cross-linking and chain scission. This correlation is fitted with the function Eq. 8 which is the same as Eq. 7 except for the x-axis shift corresponding to the elastic indentation modulus of the virgin polymer :

$$\Delta E^*_{ab}(E_i) = a\left(1 - e^{-b(E_i-4)^c}\right) \tag{8}$$

with $a = 80$, $b = 1.3$ and $c = 0.5$ as the three adjustable parameters. The link between the indentation modulus and color change is not established; nevertheless, a similar shape to the first correlation is noticed, so the same fitted function is used.

This second correlation enables the estimation of local mechanical properties without the necessity of conducting mechanical tests, as the material is characterized under the reference. Therefore, indentation modulus can be estimated in areas where measurement would be difficult, such as on rough or inclined surfaces.

5. Color images based measurement validation

This part validates the equivalence between time, temperature and pressure of thermo-oxidation, the equivalent time t^* and therefore the shift factor and the estimation of indentation modulus from a color measurement.

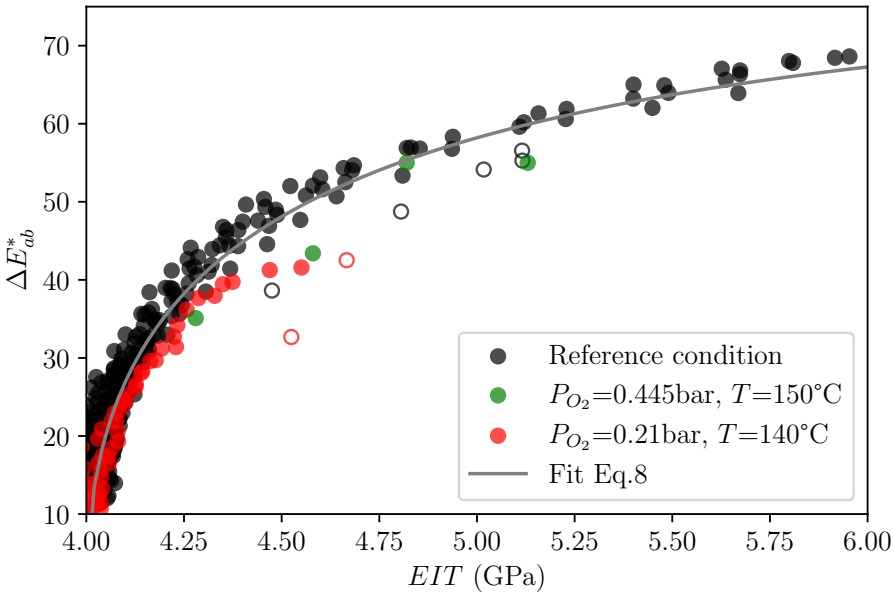

Figure 14: Relationship between color difference ΔE^*_{ab} and indentation modulus E_i at different exposure conditions of temperature T and oxygen partial pressure P_{O_2}. The black dot are obtained after aging in reference conditions. Colored dot are from sample aged in other temperature or pressure condition. The points closest to the edge are unfilled because they are subject to the edge effect (discussed later), which falsifies the measurement. The reference conditions are : $P_{O_2} = 0.21\,\text{bar}$ and $T = 150\,°\text{C}$.

5.1. Validation of equivalence between time, temperature and oxygen partial pressure

Fig. 14 aims to validate the equivalence between time, temperature and pressure. For the same oxidation level reached (under any aging condition : time, temperature, or pressure), the properties of the polymer are the same. In this figure, the black dots are the one used in the correlation in the previous part (aged in reference conditions and plotted in Fig. 13). The

colored dot is obtained from other aging conditions : the red one is for lower temperature (140 °C) but the same pressure, and the green dot is for the same temperature but higher partial pressure of oxygen (0.445 bar). When the temperature and the pressure conditions change, the exposure time must also be adjusted to obtain the same aged level. Since all the dot for different conditions are on the same master curve, this shows the equivalence between time, temperature and pressure. It is important to note that when the temperature or pressure is altered in the context of diffusion-limited oxidation, the shape of the thermo-oxidation profile will differ due to the modification of the competition between chemical kinetics and oxygen diffusion. A few points are off the master curve, they correspond to measurement points (unfilled in the plots) subject to edge effects on both color measurement and indentation measurement. Eventually, when a certain oxidation is reached, it corresponds to a unique value of color difference ΔE^*_{ab} and elastic indentation modulus E_i regardless of the surrounding aging conditions or position within the sample.

This equivalence has been validated for two temperatures based on spectrometric measurements. As illustrated in Fig. 5, the maximum of emission variation was shown to be independent of the oxidation temperature.

Finally, it is possible to use the correlation Eq. 8 established for the sample aged in the reference condition to characterize oxidation in samples aged in other conditions while the equivalence between time, temperature and pressure is valid ([49]).

5.2. Validation of the parameter equivalent time t^*

The purpose of this section is to evaluate the precision of the equivalent time parameter, t^*, as an oxidation parameter.

The equivalent time can be expressed by the product of the exposure time t and a shift factor a_T (Eq. 6). Thus, when the aging is done in different exposure conditions than the reference ones, the shift factor can be estimated to quantify the acceleration or the slowdown of the aging. Fig. 15 shows the estimation of the shift factor for samples aged in two different conditions. The gray dots are the ones used to establish the correlation Eq. 7. The shift factors have been adjusted to obtain an equivalent time such that all the color differences fit the correlation Eq. 7 established previously. The samples aged at lower temperature but the same partial pressure shows a slowdown ($a_T < 1$: equivalent to a shorter exposure time in the reference conditions), while samples aged at higher partial pressure but the same temperature accelerates the aging ($a_T > 1$: equivalent to a longer exposure time in the reference conditions).

Then, the estimation of the equivalent time t^* measurements was performed on three validation samples aged 30 h, 70 h, and 110 h under reference conditions because these are the only aging conditions where the equivalent time is known (it should be the aging duration). These samples were not used to establish the color difference - time correlation.

The estimated equivalent time t^* is presented in Fig. 16 for the three validation samples with a histogram to visualize the mean and standard deviation of the parameter t^*. The histogram was generated in the same way as in Fig. 8b.

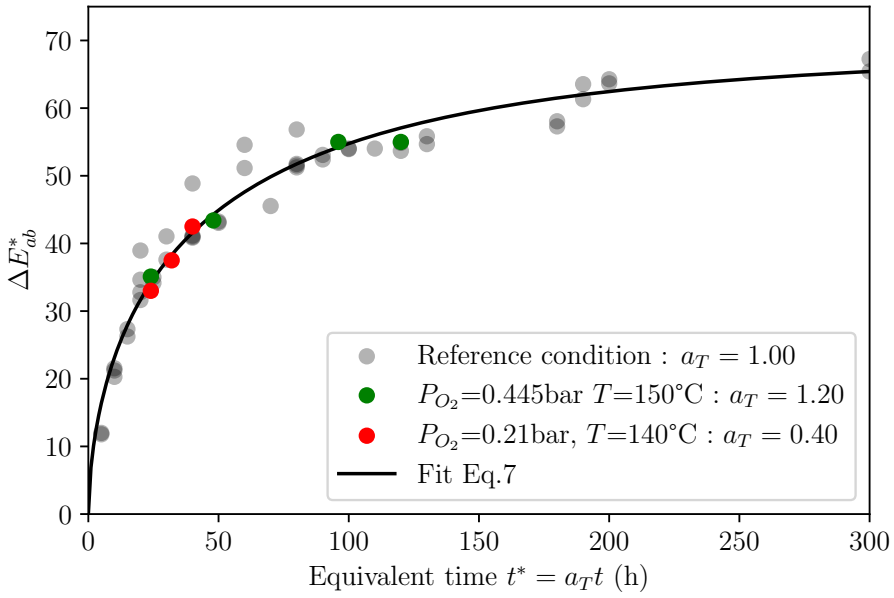

Figure 15: Shift factor estimation for samples aged at different conditions than reference ones. A slowdown occurs when $a_T < 1$ and an accelerating aging when $a_T > 1$. The reference conditions are : $P_{O_2} = 0.21\,\text{bar}$ and $T = 150\,°\text{C}$.

The width of the distribution, i.e. the standard deviation, increases with the equivalent time t^* because the calibration correlation (shown Fig. 12, fitted with the Eq.7) is not linear and its variation decreases rapidly with increasing equivalent time t^*. The spectrometer study already demonstrated that this lighting condition provides a sensitive range up to 300 h.

Tab. 2 shows the deviation between the expected values (exposure time) and the estimated t^*. A maximum deviation of 15 % is observed, which validates the method and the parameter.

Fig. 17 illustrates three oxidized layers inside aged samples obtained from

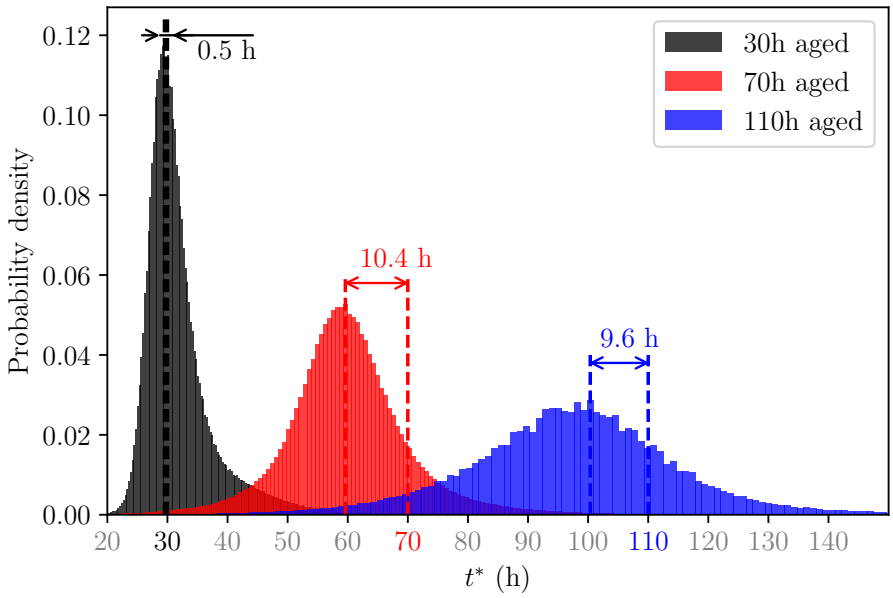

Figure 16: t^* distribution for 30 h, 70 h and 110 h aged sample. The colored x-axis label is the aged duration of each sample. The vertical dashed line shows the absolute error of the method on this three validation samples.

	30 h aged	70 h aged	110 h aged
t^* (h)	29.5	59.6	100.7
Relative error (%)	1.7	14.8	8.7

Table 2: Validation of equivalent time t^* as a quantitative oxidation parameter on homogeneous surface.

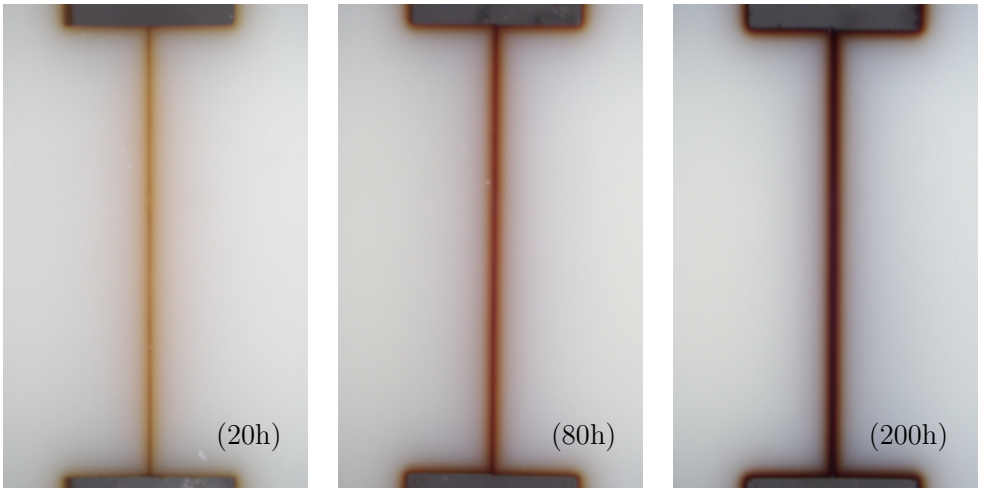

Figure 17: Images of the oxidized layer for three aging durations : 20 h, 80 h and 200 h. As the duration increases, the color change and the oxidized layer thickness increase.

a cross-section perpendicular to the surface. Color difference profiles were obtained from thick samples aged at high temperatures where chemical reactions are faster than oxygen diffusion, resulting in the creation of an oxidized layer. From the color difference profile, the equivalent time can be estimated in the oxidized layer. The equivalent time value at the edge should be the exposure time as the samples were aged in the reference conditions.

Fig. 18 shows the equivalent time t^* in function of the depth in the sample (distance from the edge). The error bars shown are obtained by propagating the color difference standard variation with the calibration correlation. (Eq. 7).

Tab. 3 summarizes the equivalent time t^* estimates with the calibration correlation. Significant estimation errors can be noticed, with error rates between 25 % and 50 %. This is due to the light scattering inside the sample.

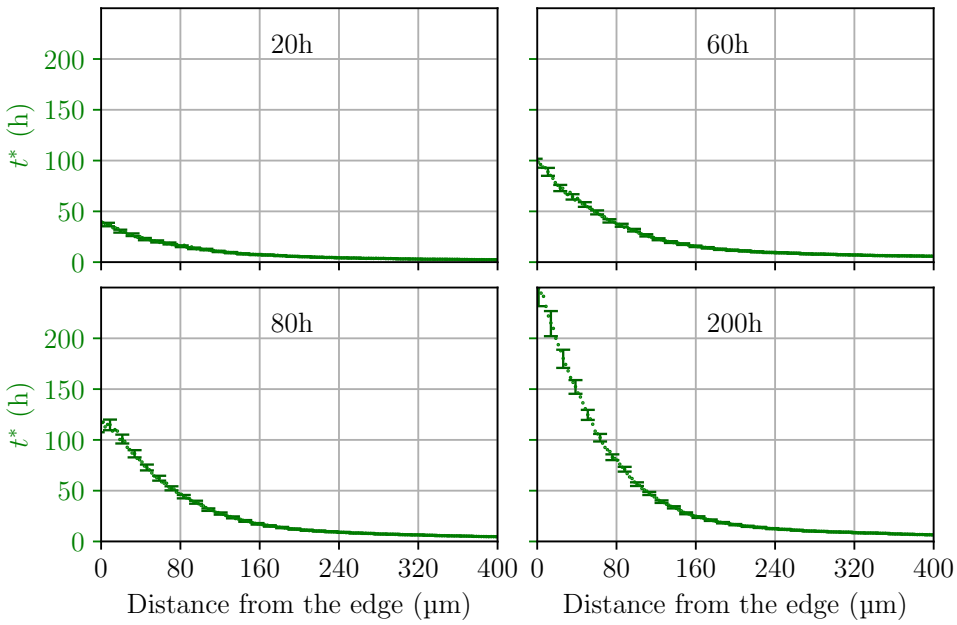

Figure 18: Equivalent time t^* inside oxidized layer of samples aged at 150 °C

The assumption is a null transmissivity is invalid here. The correlation Eq. 7 is based on homogeneous oxidized surface, while the estimation of the equivalent time inside the oxidized layer is performed in a gradient color zone. Light diffusion inside the sample differs. This figure shows the main limitation of the method as it is sensitive to the color measurement. It is recommended to establish a second correlation with the diffusion limited oxidation (DLO) presented by the sample, or to apply post-processing correction to compensate for the discrepancy. It is possible to apply a correction factor on the color difference - time correlation (Eq. 7).

Nevertheless, the equivalent time t^* can be used as a quantitative estimator for thermo-oxidation as the prediction is relatively good.

Aging duration	t^*	t^*_{min}	t^*_{max}
20 h	33 h	32 h	35 h
60 h	98 h	95 h	102 h
80 h	118 h	113 h	123 h
200 h	251 h	235 h	270 h

Table 3: Comparison between aging duration and prediction based on the correlation correlation. t^*_{min} and t^*_{max} values are obtained by propagating the standard deviation of color difference ΔE^*_{ab} (Fig.18).

5.3. Estimation of indentation elastic modulus E_i from a color difference ΔE^*_{ab} measurement

The estimation of indentation modulus from the color difference measurements by using the correlation (Eq. 8) will be validated on oxidized layer (Illustrated in Fig. 17). Indentation measurements have been done on the same sample to estimate the error induced by the method.

Fig. 19 shows the indentation modulus profile inside a sample aged at 140 °C at atmospheric conditions estimated from the color difference measurement and the correlation established by Eq.8 (black line) and measured (green dot). There is a gradient of values from the edge to the bulk of the sample. In the bulk, the elastic indentation modulus is equal to the elastic indentation modulus of the virgin sample ($E_{i_0} = 4.0\,\text{GPa}$). The degree of oxidation is higher where the sample is stiffer, close to the edge and decreases deeper. Similar variation is noticed between estimation and experimental data with a very good prediction except near the edge where the light is scattered which smooths the sharp color variation. The error (Eq. 9) is lower

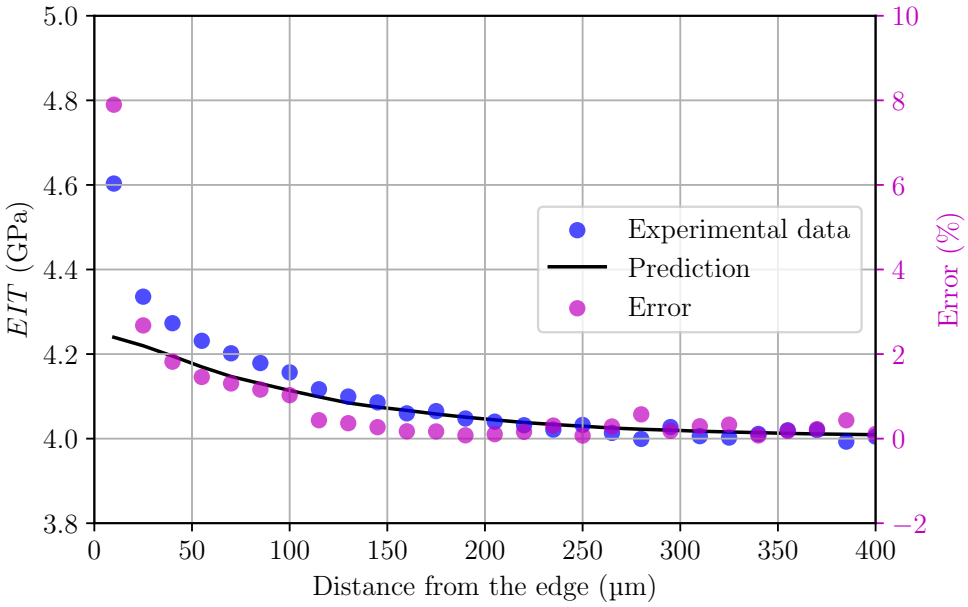

Figure 19: Measured indentation modulus (green dot) compare to the estimation of the modulus from the color difference (black line). The red dot shows the relative error from the estimation.

than 5 % except at the edge, which validates the use of color measurement as an estimator of mechanical properties.

$$Error = \frac{|E_{i_{estimated}} - E_{i_{experimental}}|}{E_{i_{experimental}}} \tag{9}$$

This validation shows that mechanical properties prediction can be done from a color measurement.

5.4. Limitations of the method

The color difference has proven to be a good method to characterize thermal oxidation. It is easier and faster to perform the measurements because it is only an image of the sample and a non-destructive measurement. The use of calibration curves eliminates the other major weakness of dependence on illumination and makes the quantity easy to understand and possible to link to more classical parameters such as the indentation modulus, which is widely used. However, the method has limitations:

- Environmental exposure conditions, validity range : The use of the correlations is not longer valid if the equivalence between time, temperature and pressure is invalid. It is of particular importance to pay close attention to the effects of high temperatures, as the chemical mechanisms of thermo-oxidation may undergo changes or become coupled with other phenomena. At low temperatures, such as room temperature, other effects such as humidity aging may invalidate the equivalence. This point will not be discussed further in this article, please refer to [49] for example.

- High oxidation level quantification : It is not suitable for characterizing high levels of oxidation and therefore long aging times. As shown in the spectroscopic study, with the LED illumination used, the absorbance does not vary beyond 300 h for samples aged in the reference conditions. If the color change is very slight, uncertainties are more significant than the quantity value, and the method must be used with caution. To focus on high oxidation levels, it is possible to utilize an optical filter or a special camera with sensitivity in the near infrared.

- Light scattering in areas with strong color gradient: The samples allow light penetration because they are not opaque. Consequently, the light scattered within affects the color measurement. Between a measurement made on a homogeneous surface (all neighboring pixels have the same color) and a heterogeneous surface (DLO, neighbors of different color), color difference can vary. To limit this undesirable effect, it is advisable to perform correlations on samples as close as possible to practical use or to apply correction.

More generally, the color measurement itself can have variations (common limitations with other characterization methods) due to :

- the roughness effect. As discussed earlier, the light reflection on the roughness of a small surface affects the standard deviation of the color difference ΔE^*_{ab}.

- the material. Two different samples may have a color difference even when they are in the virgin state. This is due to the processing step

before aging and local material composite variation. This variation has been measured to be $\Delta E^*_{ab} < 2$ which is within human eye sensitivity.

One last point is the uncertainty about the exposure time. This point is rarely discussed, but for short exposure times, the heating time can affect the real aging duration. The simplified energy balance is: $\rho C_p V \frac{\Delta T}{\Delta t} = hS\Delta T$ where ρ is the density, C_p is the heat capacity, V is the volume, T is the temperature, Δt is the heating time, h is the heat transfer coefficient, and S is the exchange surface area. The time constant is estimated : $\Delta t \approx 4\,\text{min}$. The sample will be at 95 % of the aging temperature in 12 min. For example, for 20 h aged sample, the exposure time error is 1 %.

6. Conclusion

A novel approach to thermo-oxidation characterization has been investigated based on the color change.

During thermo-oxidation, chemical modification gives rise to the formation of new chemical function groups, which in turn modify the mechanical and chemical properties of the material, including color and elastic properties. Spectrometric measurement demonstrates that these modifications are independent of the light source, with the sensitivity of the measurement range varying according to the light source in use. The primary challenge associated with spectroscopy measurements pertains to the spatial resolution and position accuracy. Subsequently, a novel methodology based on color difference is proposed as a means of circumventing this inherent limitation of spectroscopy.

From an image (or any color measurement) done with an optical microscope (or any camera), a color difference is estimated by comparing the color coordinate with a reference. The quantified thermal oxidation method is then based on calibration correlations that allow the color difference to be related to an equivalent exposure time or any mechanical parameter, here the elastic indentation modulus. These correlations are established by measuring the color difference of samples aged in reference condition for different duration. The principal benefit of utilising this calibration correlation is that it permits the manipulation of a physical quantity that is not contingent upon the specific experimental configuration.

Moreover, this characterization is a non-destructive method that can be employed *in situ* while optical access is available. Furthermore, this study has demonstrated significant time savings and a simplification of the experimental set-up, rendering it applicable to industrial parts.

However, two of the remaining limitations are the light scattering which smooths out sharp color changes and the validity of time-temperature-pressure equivalence. Edge effects also are present in nanoindentation. It is recommended that caution be exercised, as the method's sensitivity range is inherently dependent on lighting conditions.

This methodology may be generalized to any material exhibiting a relevant color change during the aging process.

Declaration of competing interest

The authors declare that they have no known competing financial interests or personal relationships that could have appeared to inuence the work

reported in this paper.

CRediT authorship contribution statement

Aurlien Doriat: Conceptualization, Investigation, Formal analysis, Methodology, Writing - original draft. **Marco Gigliotti:** Funding acquisition, Supervision, Validation, Writing - review & editing. **Marianne Beringhier:** Funding acquisition, Supervision, Validation, Writing - review & editing. **Gildas Lalizel:** Funding acquisition, Supervision, Validation, Writing - review & editing. **Eva Dorignac:** Supervision, Validation, Writing - review & editing. **Patrick Berterretche:** Conceptualization, Supervision, Writing - review & editing. **Matteo Minervino:** Funding acquisition, Writing - review & editing.

Acknowledgments

This work was supported by the French government program "Investissements d'Avenir" (EUR INTREE, reference ANR-18-EURE-0010). This work pertains to the French government program "Investissements d'Avenir" (LABEX INTERACTIFS, reference ANR-11-LABX-0017-01). Herv Arlaud is thanked for his help with imaging and for providing the microscope. The authors thank SAFRAN Aircraft Engines for providing the polymer material.

References

[1] F.-L. Jin, X. Li, S.-J. Park, Synthesis and application of epoxy resins: A review, J. Ind. Eng. Chem. 29 (2015) 1–11. doi:10.1016/j.jiec.2015.03.026.

[2] P.-S. Shin, J.-H. Kim, H.-S. Park, Y.-M. Baek, S.-I. Lee, K. L. DeVries, J.-M. Park, A review: Mechanical and interfacial properties of composites after diverse types of aging using micromechanical evaluation, Fiber. Polym. 21 (2) (2020) 225–237. doi:10.1007/s12221-020-9700-7.

[3] J. L. Down, The yellowing of epoxy resin adhesives: Report on high-intensity light aging, Stud. Conserv. 31 (4) (1986) 159–170. doi:10.2307/1506247.

[4] C. Wu, B. C. Meng, L.-h. Tam, L. He, Yellowing mechanisms of epoxy and vinyl ester resins under thermal, uv and natural aging conditions and protection methods, Polym. Test. 114 (2022) 107708. doi:10.1016/j.polymertesting.2022.107708.

[5] M. Celina, J. Wise, D. K. Ottesen, K. T. Gillen, R. L. Clough, Correlation of chemical and mechanical property changes during oxidative degradation of neoprene, Polym. Degrad. Stab. 68 (2) (2000) 171–184. doi:10.1016/S0141-3910(99)00183-4.

[6] N. Rasoldier, X. Colin, J. Verdu, M. Bocquet, L. Olivier, L. Chocinski-Arnault, M. C. Lafarie-Frenot, Model systems for thermo-oxidised epoxy composite matrices, Compos. Part A-Appl. S. 39 (9) (2008) 1522–1529. doi:10.1016/j.compositesa.2008.05.016.

[7] S. Terekhina, M. Mille, B. Fayolle, X. Colin, Oxidation induced changes in viscoelastic properties of a thermostable epoxy matrix, Polym. Sci. Ser. A+ 55 (10) (2013) 614–624.

[8] E. Ernault, E. Richaud, B. Fayolle, Origin of epoxies embrittlement during oxidative ageing, Polym. Test. 63 (2017) 448–454. doi:10.1016/j.polymertesting.2017.09.004.

[9] T. Ishida, E. Richaud, M. Gervais, A. Gaudy, R. Kitagaki, H. Hagihara, Y. Elakneswaran, Thermal aging of acrylic-urethane network: Kinetic modeling and end-of-life criteria combined with mechanical properties, Prog. Org. Coat. 163 (2022) 106654. doi:10.1016/j.porgcoat.2021.106654.

[10] G. Schoeppner, G. Tandon, K. Pochiraju, Predicting thermooxidative degradation and performance of high-temperature polymer matrix composites, in: Multiscale modeling and simulation of composite materials and structures, Springer, 2008, pp. 359–462.

[11] B. Fayolle, X. Colin, L. Audouin, J. Verdu, Mechanism of degradation induced embrittlement in polyethylene, Polym. Degrad. Stab. 92 (2) (2007) 231–238. doi:10.1016/j.polymdegradstab.2006.11.012.

[12] B. Mailhot, P.-O. Bussière, A. Rivaton, S. Morlat-Thérias, J.-L. Gardette, Depth profiling by afm nanoindentations and micro-ftir spectroscopy for the study of polymer ageing, Macromol. rapid comm. 25 (2) (2004) 436–440.

[13] L. Olivier, N. Q. Ho, J. C. Grandidier, M. C. Lafarie-Frenot, Characterization by ultra-micro indentation of an oxidized epoxy polymer: Correlation with the predictions of a kinetic model of oxidation, Polym.

Deg. Stab. 93 (2) (2008) 489–497. doi:10.1016/j.polymdegradstab.2007.11.012.

[14] M. C. Lafarie-Frenot, J. C. Grandidier, M. Gigliotti, L. Olivier, X. Colin, J. Verdu, J. Cinquin, Thermo-oxidation behaviour of composite materials at high temperatures: A review of research activities carried out within the comedi program, Polym. Degrad. Stab. 95 (WOS:000278750800010) (2010) 965–974. doi:10.1016/j.polymdegradstab.2010.03.019.

[15] J.-F. Larché, P.-O. Bussière, S. Thérias, J.-L. Gardette, Photooxidation of polymers: Relating material properties to chemical changes, Polym. Degrad. Stab. 97 (1) (2012) 25–34. doi:10.1016/j.polymdegradstab.2011.10.020.

[16] J. C. Grandidier, L. Olivier, M. C. Lafarie-Frenot, M. Gigliotti, Modeling the pressure dependent solubility in a thermoset resin for simulating pressure accelerated thermo-oxidation tests, Mech. Mater. 84 (WOS:000352751400004) (2015) 44–54. doi:10.1016/j.mechmat.2014.09.008.

[17] M. Gigliotti, M. Minervino, M. C. Lafarie-Frenot, Assessment of thermo-oxidative induced chemical strain by inverse analysis of shrinkage profiles in unidirectional composites, Compos. Struct. 157 (2016) 320–336. doi:10.1016/j.compstruct.2016.07.037.

[18] M. Pecora, O. Smerdova, M. Gigliotti, Gradients of cyclic indentation mechanical properties in pr520 epoxy and its 3d carbon fiber composite

induced by aging at 150 °c, Polym. Degrad. Stab. 193 (2021) 109720. doi:10.1016/j.polymdegradstab.2021.109720.

[19] L. Audouin, V. Langlois, J. Verdu, J. De Bruijn, Role of oxygen diffusion in polymer ageing: kinetic and mechanical aspects, J. Mater. Sci. 29 (3) (1994) 569–583.

[20] G. Mertz, F. Hassouna, P. Leclère, A. Dahoun, V. Toniazzo, D. Ruch, Correlation between (nano)-mechanical and chemical changes occurring during photo-oxidation of filled vulcanised styrene butadiene rubber (sbr), Polym. Deg. Stab. 97 (11) (2012) 2195–2201. doi:10.1016/j.polymdegradstab.2012.08.008.

[21] P. Y. Le Gac, M. Celina, G. Roux, J. Verdu, P. Davies, B. Fayolle, Predictive ageing of elastomers: Oxidation driven modulus changes for polychloroprene, Polym. Degrad. Stab. 130 (2016) 348–355. doi:10.1016/j.polymdegradstab.2016.06.014.

[22] S. Eibl, Comparison of surface and bulk analytical techniques for the distinct quantification of a moderate thermal pre-load on a carbon fibre reinforced plastic material, Polym. Degrad. Stab. 135 (2017) 31–42. doi:10.1016/j.polymdegradstab.2016.11.015.

[23] S. Konica, T. Sain, A reaction-driven evolving network theory coupled with phase-field fracture to model polymer oxidative aging, J. Mech. Phys. Solids 150 (2021) 104347. doi:10.1016/j.jmps.2021.104347.

[24] S. Putthanarat, G. Tandon, G. Schoeppner, Influence of polishing time on thermo-oxidation characterization of isothermally aged pmr-

15 resin, Polym. Deg. Stab. 92 (11) (2007) 2110–2120. doi:10.1016/j.polymdegradstab.2007.07.007.

[25] G. Z. Voyiadjis, A. Samadi-Dooki, L. Malekmotiei, Nanoindentation of high performance semicrystalline polymers: A case study on peek, Polym. Test. 61 (2017) 57–64. doi:10.1016/j.polymertesting.2017.05.005.

[26] J. L. Loubet, J. M. Georges, G. Meille, Vickers indentation curves of elastoplastic materials. (1985).

[27] W. C. Oliver, G. M. Pharr, Improved technique for determining hardness and elastic modulus using load and displacement sensing indentation experiments (1992).

[28] J. Woirgard, J.-C. Dargenton, An alternative method for penetration depth determination in nanoindentation measurements, J. Mater. Res. 12 (9) (1997) 2455–2458. doi:10.1557/JMR.1997.0324.

[29] D. Rosu, L. Rosu, C. N. Cascaval, Ir-change and yellowing of polyurethane as a result of uv irradiation, Polym. Degrad. Stab. 94 (4) (2009) 591–596. doi:10.1016/j.polymdegradstab.2009.01.013.

[30] A. Rivaton, L. Moreau, J.-L. Gardette, Photo-oxidation of phenoxy resins at long and short wavelengths–i. identification of the photo-products, Polym. Deg. Stab. 58 (3) (1997) 321–332. doi:10.1016/S0141-3910(97)00089-X.

[31] B. Mailhot, S. Morlat-Thérias, M. Ouahioune, J.-L. Gardette, Study of

the degradation of an epoxy/amine resin, 1, Macromol. Chem. Phys. 206 (5) (2005) 575–584. doi:10.1002/macp.200400395.

[32] A. E. Krauklis, A. T. Echtermeyer, Mechanism of yellowing: Carbonyl formation during hygrothermal aging in a common amine epoxy, Polymers 10 (9) (2018). doi:10.3390/polym10091017.

[33] M. C. Celina, E. Linde, E. Martinez, Carbonyl identification and quantification uncertainties for oxidative polymer degradation, Polym. Deg. Stab. 188 (2021) 109550. doi:10.1016/j.polymdegradstab.2021.109550.

[34] N. S. Allen, M. Edge, S. Hussain, Perspectives on yellowing in the degradation of polymer materials: inter-relationship of structure, mechanisms and modes of stabilisation, Polym. Degrad. Stab. 201 (2022) 109977. doi:10.1016/j.polymdegradstab.2022.109977.

[35] Y. Ni, T. T. Bisel, M. P. Spencer, W. K. Fuchs, M. R. Pallaka, L. S. Fifield, IEEE, Color change during thermal degradation of polyolefin electric cable insulations (2021).

[36] M. Spencer, W. Fuchs, Y. Ni, D. Li, M. R. Pallaka, A. Arteaga, L. S. Fifield, Color as a tool for quantitative analysis of heterogeneous polymer degradation, Mater. Today Chem. 29 (2023) 101417. doi:10.1016/j.mtchem.2023.101417.

[37] M. S. Oliveira, A. C. Pereira, H. A. Colorado, N. M. Meliande, J. D. da Cunha, A. B. Figueiredo, S. N. Monteiro, Thermal and colorimetric

parameter evaluation of thermally aged materials: A study of diglycidyl ether of bisphenol a/triethylenetetramine system and fique fabric-reinforced epoxy composites (2023). doi:10.3390/polym15183761.

[38] P. B. Stickler, M. Ramulu, Investigation of mechanical behavior of transverse stitched t-joints with pr520 resin in flexure and tension, Compos. Struct. 52 (3) (2001) 307–314. doi:10.1016/S0263-8223(01)00023-X.

[39] X. Colin, F. Essatbi, J. Delozanne, G. Moreau, Towards a general kinetic model for the thermal oxidation of epoxy-diamine networks. effect of the molecular mobility around the glass transition temperature, Polym. Degrad. Stab. 181 (109314) (2020). doi:10.1016/j.polymdegradstab.2020.109314.

[40] P. Hao, S. W. F. Spronk, W. Van Paepegem, F. A. Gilabert, Hydraulic-based testing and material modelling to investigate uniaxial compression of thermoset and thermoplastic polymers in quasistatic-to-dynamic regime, Mater. Des. 224 (2022) 111367. doi:10.1016/j.matdes.2022.111367.

[41] M. Minervino, Effets de la thermo-oxydation sur le comportement mécanique de matériaux composites pour applications aéronautiques, Theses, ISAE-ENSMA Ecole Nationale Supérieure de Mécanique et d'Aérotechique - Poitiers (Nov. 2013).

[42] M. C. Celina, A. R. Dayile, A. Quintana, A perspective on the inherent oxidation sensitivity of epoxy materials, Polymer 54 (13) (2013) 3290–3296. doi:10.1016/j.polymer.2013.04.042.

[43] K. T. Gillen, R. Bernstein, M. Celina, Challenges of accelerated aging techniques for elastomer lifetime predictions (2015). doi:10.5254/rct.14.85930.

[44] P. Gijsman, W. F. Dong, A. Quintana, M. Celina, Influence of temperature and stabilization on oxygen diffusion limited oxidation profiles of polyamide 6 (2016). doi:10.1016/j.polymdegradstab.2016.05.024.

[45] M. Celina, E. Linde, D. Brunson, A. Quintana, N. Giron, Overview of accelerated aging and polymer degradation kinetics for combined radiation-thermal environments, Polym. Degrad. Stab. 166 (2019) 353–378.

[46] H. L. McManus, R. A. Cunningham, Coupled materials and mechanics analyses of durability tests for high temperature polymer matrix composites, ASTM STP 1302 (1995) 1–17.

[47] K. Chrissafis, Kinetics of thermal degradation of polymers, J. Therm. Anal. Calorim. 95 (1) (2009) 273–283.

[48] X. Colin, F. Essatbi, J. Delozanne, G. Moreau, A new analytical model for predicting the thermal oxidation kinetics of composite organic m atrices. application to diamine cross-linked epoxy, Polym. Degrad. Stab. 186 (2021) 109513.

[49] M. C. Celina, Review of polymer oxidation and its relationship with materials performance and lifetime prediction, Polym. Degrad. Stab. 98 (12) (2013) 2419–2429.

Declaration of interests

The authors declare that they have no known competing financial interests or personal relationships that could have appeared to influence the work reported in this paper.

The authors declare the following financial interests/personal relationships which may be considered as potential competing interests:

Graphical Abstract

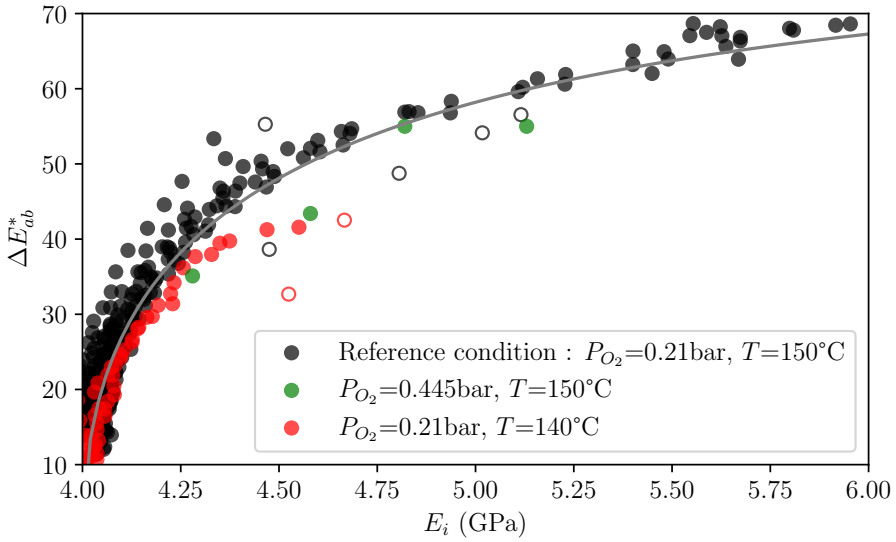

The color measurement ΔE^*_{ab} and the mechanical property E_i are analogous.
Once a correlation is established in reference conditions (T=150°C and $P = 0.21bar$),
any other aging conditions (colored dots) follow the same correlation between these two data sets.

Highlights

- Color-based characterization method is established to quantify thermo-oxidation.
- Mechanical properties are estimated from color difference measurements.
- An equivalent time t^* parameter is defined and compared to indentation measurements.
- t^* indicates aging time needed in the reference conditions to match oxidation levels.

- The equivalent time helps providing a quick estimation of oxidation acceleration.